Disuse-driven plasticity in the human thalamus and putamen

Roselyne J. Chauvin[1,✉], Dillan J. Newbold[2], Ashley N. Nielsen[1], Ryland L. Miller[3], Samuel R. Krimmel[1], Athanasia Metoki[1], Anxu Wang[1,4], Andrew N. Van[1,5], David F. Montez[1,6], Vahdeta Suljic[1], Noah J. Baden[1], Nadeshka Ramirez-Perez[1], Kristen M. Scheidter[1], Julia S. Monk[1], Forrest I. Whiting[1], Babatunde Adeyemo[1], Benjamin P. Kay[1], Timothy O. Laumann[6], Evan M. Gordon[7], and Nico U.F. Dosenbach[1,4,6,8]

[1] Department of Neurology, Washington University School of Medicine, St. Louis, MO 63110
[2] Department of Neurology, New York University Grossman School of Medicine, New York, New York 10016, USA
[3] Basque Center on Cognition, Brain and Language, Donostia, Gipuzkoa, Spain
[4] Department of Biomedical Engineering, Washington University in St. Louis, MO 63130
[5] Division of Computation and Data Science, Washington University School of Medicine, St. Louis, MO 63110
[6] Department of Psychiatry, Washington University School of Medicine, St. Louis, MO 63110
[7] Mallinckrodt Institute of Radiology, Washington University School of Medicine, St. Louis, MO 63110
[8] Department of Pediatrics, Washington University School of Medicine, St. Louis, MO 63110

✉ Correspondence: Roselyne J Chauvin <chauvin@wustl.edu>

Abstract:

Cortico-striato-thalamo-cortical loops have been heavily studied because of their importance in movement disorders such as Parkinson's Disease and tremor. Capturing plasticity effect in this circuit has been mainly successful using animals or using invasive electrophysiology in patients. Given the importance of the striatum and thalamus for motor control and skill learning, the current study leverages on an arm immobilization paradigm in humans with neuroimaging to induce disuse and explore human subcortical motor circuits plasticity. We employed an experimental paradigm involving upper-extremity immobilization for two weeks with daily resting-state functional connectivity (FC) and motor task-related fMRI. This approach of dense sampling of individuals, i.e Precision Functional Mapping (PFM), offers individual-specific insights and provides enough data to address the issue of low signal to noise ratio in the subcortex. Previously, we identified increased FC between somatomotor cortex and the cingulo-opercular network and emergence of disuse pulses in the cortex during casting. We expand our prior investigation to include analysis adapted to the signal characteristic of subcortical regions to capture disuse-driven plasticity in human subcortical circuits. Subcortical nodes, particularly the central thalamus and posterior putamen, exhibited strengthened FC during disuse and spontaneous activity pulses. Motor task fMRI validated that subcortical disuse-driven plasticity effects spatially correspond to the upper extremity movement execution circuitry, emphasizing the role of these structures in motor control and adaptation. In conclusion, our study highlights the involvement of the cortico-striato-thalamo-cortical loops in human motor plasticity and discuss similarities in findings with two research fields: Parkinson Disease (PD), suggesting a novel interpretation of PD neuroimaging finding; and sleep, particularly plasticity and sleep pressure regulated by the thalamus.

Intro

Brain networks must exhibit the dual characteristics of stability, to preserve rarely used skills, and flexibility, to adapt to environmental changes and acquire new abilities[1]. Behavior, manifested as movement, is generated by complex cortico-subcortical circuits including the thalamus, basal ganglia and cerebellum. Cortico-striato-thalamo-cortical loops have been heavily studied because of their importance in movement disorders such as Parkinson's disease and tremor. Capturing plasticity effect in this circuit has been mainly successful with focal electrophysiology in patients undergoing clinical interventions (i.e. deep brain stimulation [DBS])[2–4], or animals[5,6]. Human neuroimaging studies have often captured effects on cortex, while experiencing difficulty to obtain significant results in subcortex, due to its lower signal to noise ratio[7,8], especially in plasticity paradigms, given their small effect sizes[9–11].

To study plasticity mechanisms in humans, we developed an experimental paradigm that induces disuse by restraining the upper-extremity in a full length cast [12–14]. This approach is similar to classical animal plasticity studies, which impose motor or sensory restrictions (e.g., limb constraint, deafferentation, monocular deprivation) in a small number of intensively studied individuals [15,16]. We casted the dominant upper extremity of three participants (Nico, Ashley and Omar) for two weeks and collected high density data with around-the-clock movement actigraphy and daily functional MRI (fMRI) sessions (resting state functional connectivity [FC]; motor task fMRI) for 6-8 weeks (2 weeks prior casting as baseline and 2-4 weeks of follow up). After casting, accelerometer data worn on both wrists quantified a reduction of the use of the dominant arm to the profit of the non dominant arm. After removing the cast however, no motor skill impairment was observed, except for a rapidly recovered reduction of grip strength (1 to 7 days). FC noninvasively maps the brain's functional networks and how they change in response to disuse. Dense longitudinal sampling, enabled us to perform within participant analyses using our individual-specific Precision Functional Mapping (PFM) methodology [17].

Our previous analyses of this disuse-driven plasticity PFM dataset focused on the cerebral cortex [13,14]. We first observed a large decrease in FC between the left and right effector specific upper-extremity primary somatomotor cortex ($SM1_{ue}$) (-0.23 to -0.86 change in correlation), which are ordinarily strongly coupled. We detected increased FC between left $SM1_{ue}$, controlling the casted arm, and the cingulo-opercular network (CON)[13]. The CON serves as an executive control system responsible for top-down regulation of actions, from more abstract cognition to more concrete motor plans [18,19]. After 12-48 hours of arm casting, large MRI signal fluctuations emerged in the disused motor cortex. These disuse pulses accounted for some, but not all of the increases in FC between $SM1_{ue}$ and the CON [14]. Changes in FC and emergence of disuse pulses during casting are part of the motor control circuit linking multiple functional cortical networks. We question whether the PFM approach could help disentangling how networks coordinate changes.

Our PFM approach has uncovered neuroanatomical complexities, less apparent in group-averaged data. For example, we recently described the previously unrecognized Somato-Cognitive Action network (SCAN), which is interleaved with effector-specific motor regions along the central sulcus [20]. The SCAN is strongly functionally connected to the CON, and seems to serve as its downstream actuator, turning more abstract plans into integrated whole-body actions that include not only skeletal muscle movement, but also arousal, allostatic physiological changes and control of internal organs. The discovery of SCAN provides novel context of the CON to effector-specific motor regions pathway, where the SCAN could be a mediator to the CON to motor effector change in FC during casting. This insight warrants re-evaluating our prior interpretations of some of the disuse-driven plasticity effects.

Motor control circuits cannot be understood without including subcortical nodes. Basal ganglia (putamen, caudate, globus pallidus, etc.) circuits constitute a complex network within the subcortex that is intricately structured to facilitate the selection of intended actions while simultaneously suppressing or inhibiting potentially conflicting or undesirable actions [21]. The putamen specifically has been shown to be important for both fast reward-dependent motor learning (anterior) and slow but long-term establishment of habits (posterior) [22,23]. In the context of upper extremity restraint, we expect the basal ganglia to play a role in inhibiting dominant arm movement and enhancing new motor learning behavior.

The central thalamus also plays a significant role in motor adaptation and control by serving as a relay and integration center between various brain regions involved in motor functions [24]. The thalamus comprises a multitude of distinct nuclei, including the ventroposterior lateral (VPL) and the ventralis intermedius (VIM) nuclei [25,26]. The VPL receives sensory information and relay information for fine tuning of movement. The VIM, in comparison, is primarily involved in motor control functions such as planning, initiation, and execution of voluntary movements. With negative sensory feedback due to upper extremity restraint during intent of upper arm execution, we expect these thalamic nuclei to be involved in the movement adaptation. The VIM is the deep brain stimulation (DBS) target in Essential Tremor and tremor-predominant Parkinson's Disease (PD) [27–31] . A case report from a patient with longstanding bilateral upper extremity loss undergoing DBS suggested plasticity of VIM neurons, leading to an over-representation of shoulder movements[32].

The centromedian nucleus (CM) of the thalamus, is being targeted with DBS in Tourette's Syndrome and also in epilepsy [4]. It has been classified as part of the 'non-specific' nuclei of the thalamus and shows specific projections to the sensorimotor regions and anterior cingulate [5]. The CM plays an important role in the regulation of the cortical parvalbumin neurons that promote Hebbian plasticity [33–36] , and the overall level of cortical activity and arousal [37]. CM has mainly been used for DBS in refractory generalized epilepsy [38–40] due to its role in sleep-wake regulation and arousal. The central thalamus plays an important role in regulating sleep stages and generates sleep spindles important for memory consolidation [41–43], including procedural memory, therefore we wonder if the thalamus could play a role in the emerging disuse pulse.

Given the importance of subcortical structures for motor control and skill learning, we expanded our prior analyses to investigate disuse-driven plasticity in human subcortical circuits for the first time.

Results

Disuse strengthens somatomotor cortex functional connectivity with central thalamus and posterior putamen

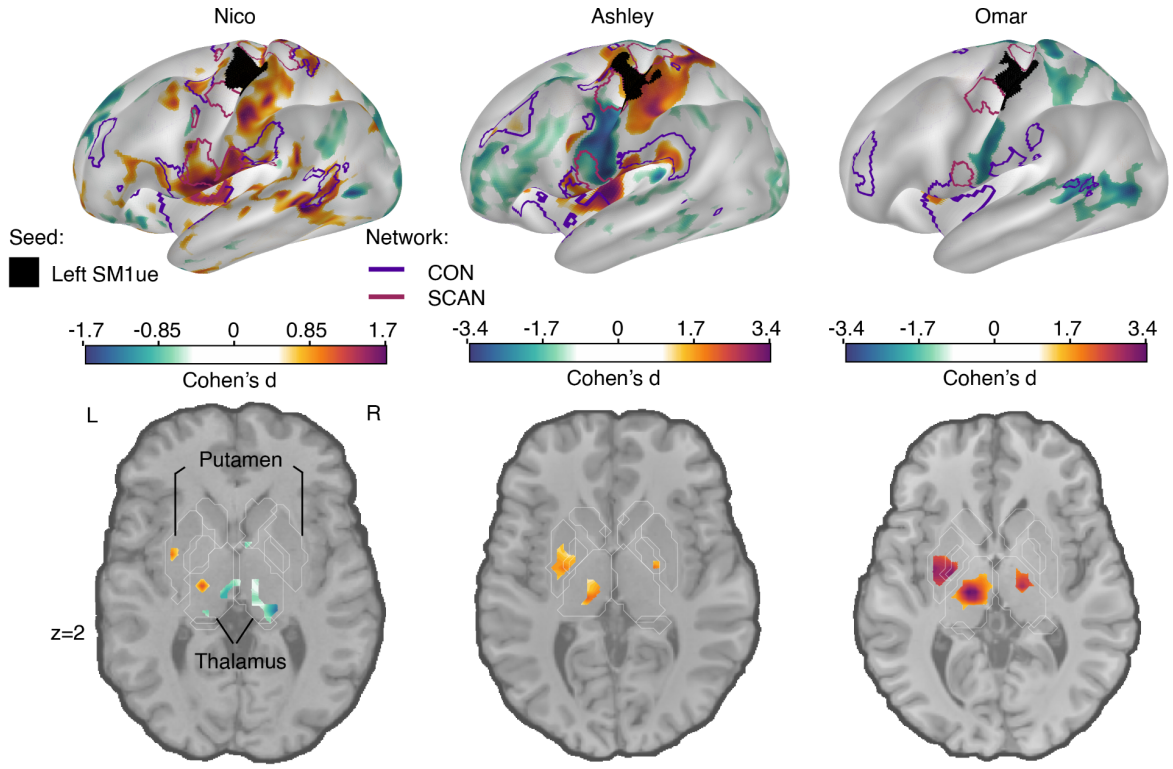

Figure 1: Disuse-driven changes in functional connectivity (FC) of effector-specific primary somatomotor cortex (L-SM1$_{ue}$). *Individual-specific plasticity effect size (Cohen's d) maps showing changes in FC during casting (Cast − Pre) for the L-SM1$_{ue}$ (black), and for each participant (left to right columns: Nico, Ashley, Omar). For reference, a Cohen's d of 0.8 is generally considered a large effect size. Only significant effects after cluster correction at $p < 0.05$ (see Methods) are displayed. With a TR that is twice as long, Nico's effect sizes are about half the size of the other participants. The functional network borders of the Cingulo-opercular (CON, purple) and Somato-cognitive action (SCAN, maroon) networks are displayed on the inflated surface rendering (top row). The freesurfer based anatomical borders of subcortical regions are overlaid on the horizontal slices.The putamen and thalamus are shown with white outlines (bottom row).*

FC in the subcortex is weaker than in cortex, because fMRI signal strength drops off towards the center of the brain, as distance from the MRI coil elements increases. Therefore, when simply subtracting the FC maps for different conditions (i.e., Cast - Pre), plasticity effects in cortex will wash out subcortical ones. To properly evaluate disuse-driven plasticity in the subcortex we therefore utilized a standardized effect size (Cohen's d), which can account for mean signal strength differences between cortex and subcortex. We computed the effect size of the FC change between the casting and pre-casting scans for the left hemisphere primary somatomotor cortex (SM1) upper extremity, related to the disuse arm (Figure 1). Use-driven FC changes (Cohen's d) of the left SM1 increases with the CON regions (purple border, figure 1) for all three participants in cortex and with hand motor regions in the cerebellum (Figure S1, S3). This result replicated the parcel-based FC changes we previously reported [13]. Furthermore, including the Somato-Cognitive Action Network (Figure 1, maroon outlines), which we recently described [20], reveals that the cortical disuse-driven FC changes are specific to CON, while sparing SCAN (see also Figure S2). Specifically, the two SCAN regions around the motor effector region (black seed region, left $SM1_{ue}$) do not show significant FC change during casting.

In the subcortex, all three participants showed statistically significant increases in FC between disused left $SM1_{ue}$ and the central thalamus, as well as the posterior putamen (Figure 1, bottom row; Table 1; cluster-based thresholding; see Methods). The amplitude of this subcortical effect is as strong as the cortical effect.

Other FC changes were significant but inconsistent across participants in other subcortical structures and therefore are not reported. For example, in Ashley and Omar, a small area of significant FC increase was observed in the left posterior globus pallidus bilaterally. Power might still be insufficient as there were brain-wide cross participant differences in effect size. Ashley and Omar's effects were roughly twice those observed in Nico. These differences are likely attributable to the higher temporal resolution (TR 1.1s Ashley, Omar vs. 2.2s Nico) in data acquisition, which increases the observation sample for detectability.

	Nico	Ashley	Omar
Left posterior Putamen	-31 -6 0 N_{vox} = 43	-25 -12 0 N_{vox} = 76	-31 -9 3 N_{vox} = 71
Left Thalamus	-16 -21 6 N_{vox} = 68	-7 -21 0 N_{vox} = 72	-13 -24 6 N_{vox} = 219

Table 1: Disuse-driven functional connectivity changes in subcortex. *Peak coordinate (x,y,z) in MNI space and cluster size (N_{vox}) for subcortical regions with disuse-driven increases in functional connectivity with L-$SM1_{ue}$.*

Disuse pulses are detected in the central thalamus and motor cerebellum

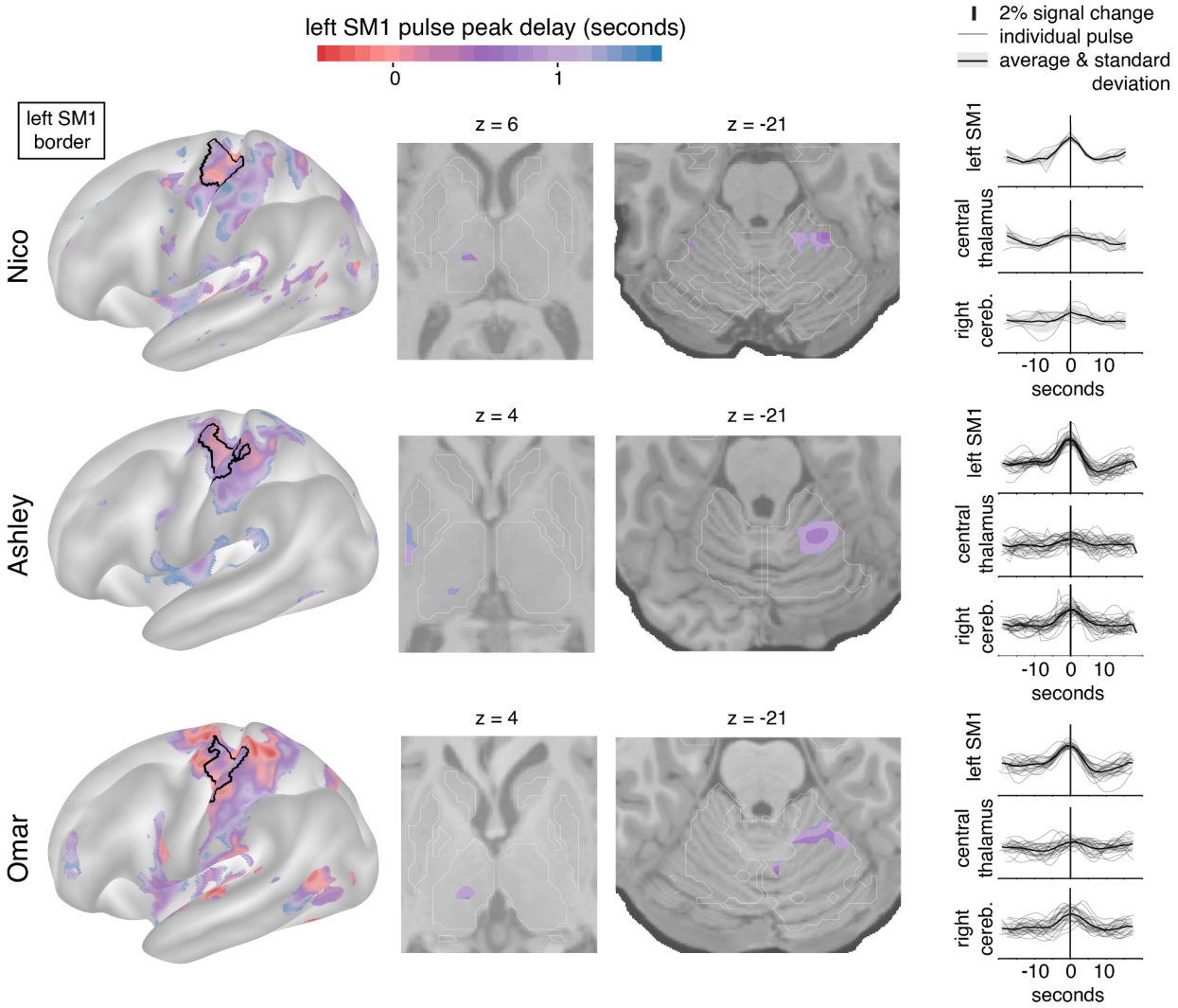

Figure 2: Disuse pulse distribution in cortex and subcortex. *The timecourse of each disuse pulse observed during casting was modeled using a Hemodynamic Response Function (HRF) (see Methods). The left hemisphere cortical surface (left), and subcortical horizontal slices (center: thalamic and cerebellar view) highlight pulses across participants (Nico, top; Ashley, middle; Omar, bottom). The color scale spans 2 seconds bracketing the average left $SM1_{ue}$ pulse peak. The maps are thresholded at the 20th percentile. The participant-specific upper extremity somatomotor region is outlined in black (left). On the right the individual (thin lines) and average (thick line) pulse timecourses are shown (y-axes: percent signal change) for the left SM1, the left thalamus and right cerebellum.*

We previously reported the emergence of large MRI signal fluctuations in the disused motor cortex after 12-48 hours of arm casting. To study the subcortical patterns of disuse pulses, we developed an HRF-based pulse detection method that is more

sensitive in the setting of weaker fMRI signals (see Methods). Using the HRF-based detection method, we were able to detect the presence of disuse pulses in the subcortex on top of confirming their spatial distribution in the cortex (Figure 2; left) and cerebellum (Figure 2; third column) [14]. Across all participants, we also observed disuse pulses in the central thalamus (Figure 2; second column). The peak pulse amplitudes in the thalamus were lower compared to cortex (Figure 2, right column), which can be dependent on the lower SNR. In the participant with the highest total number of disuse pulses throughout the brain (Ashley), we also detected them in the posterior putamen.

Disuse pulses peak across the brain with a delay. We previously demonstrated that SMA regions peak earlier than left $SM1_{ue}$, followed by the cerebellum. With our pulse detection analysis, we can define the peak delay at the vertex level during pulses. On average, the central thalamus pulses peak later than in left $SM1_{ue}$ (Figure 2; first and second columns, Nico +0.75 seconds (sd 0.16); Ashley +1.07s (sd 0.02); Omar +0.95s (sd 0.09)).

FC changes and disuse pulses overlap in the central thalamus

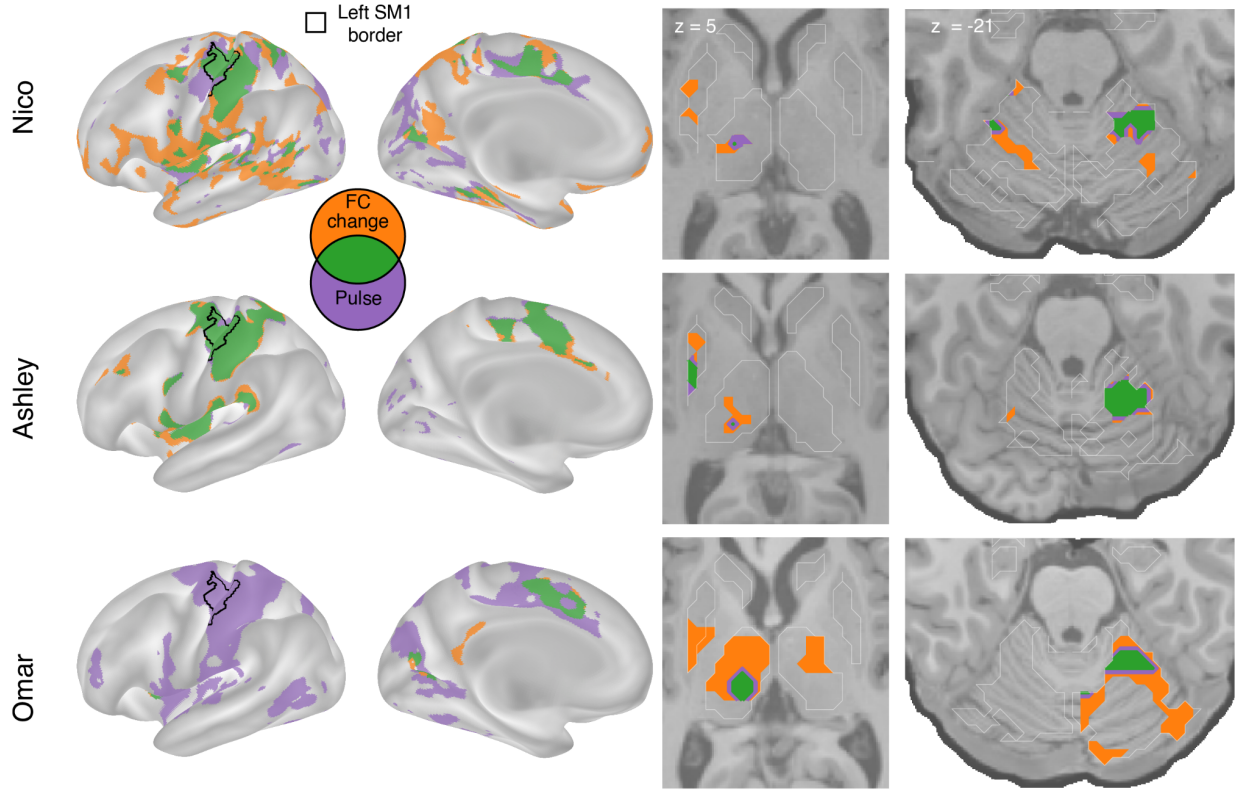

Figure 3: Spatial overlap of functional connectivity (FC) increases and disuse pulses. *The strongest disuse-driven FC increases (orange, Cast>Pre, cluster corrected) and disuse pulses (purple, top 20% threshold), as well as their overlap (green) are shown on the cortical surface (left), in the thalamus and putamen (middle) and the cerebellum (right). Results are displayed on the lateral left hemisphere surface, medial left hemisphere surface, and two horizontal slices (MNI z = 5 and -21). White borders on*

horizontal slices defined individual specific freesurfer based anatomical structures (z = 5: putamen, globus pallidus, caudate, thalamus; z = -21: cerebellum, hippocampus).

We overlapped FC changes (Figure 1) and disuse pulses (Figure 2) to visualize the spatial relationship of the two phenomena (Figure 3). All participants showed overlap (green) between disuse-driven FC changes and pulses in the dorsal medial cortex (SMA, pre-SMA, dACC), the central thalamus and the effector-specific motor regions of the cerebellum (Figure 3 and Figure S3). The participant (Ashley) that shows pulses in posterior putamen also showed overlap with FC increases.

Subcortical disuse-driven plasticity effects overlap with upper extremity task activation

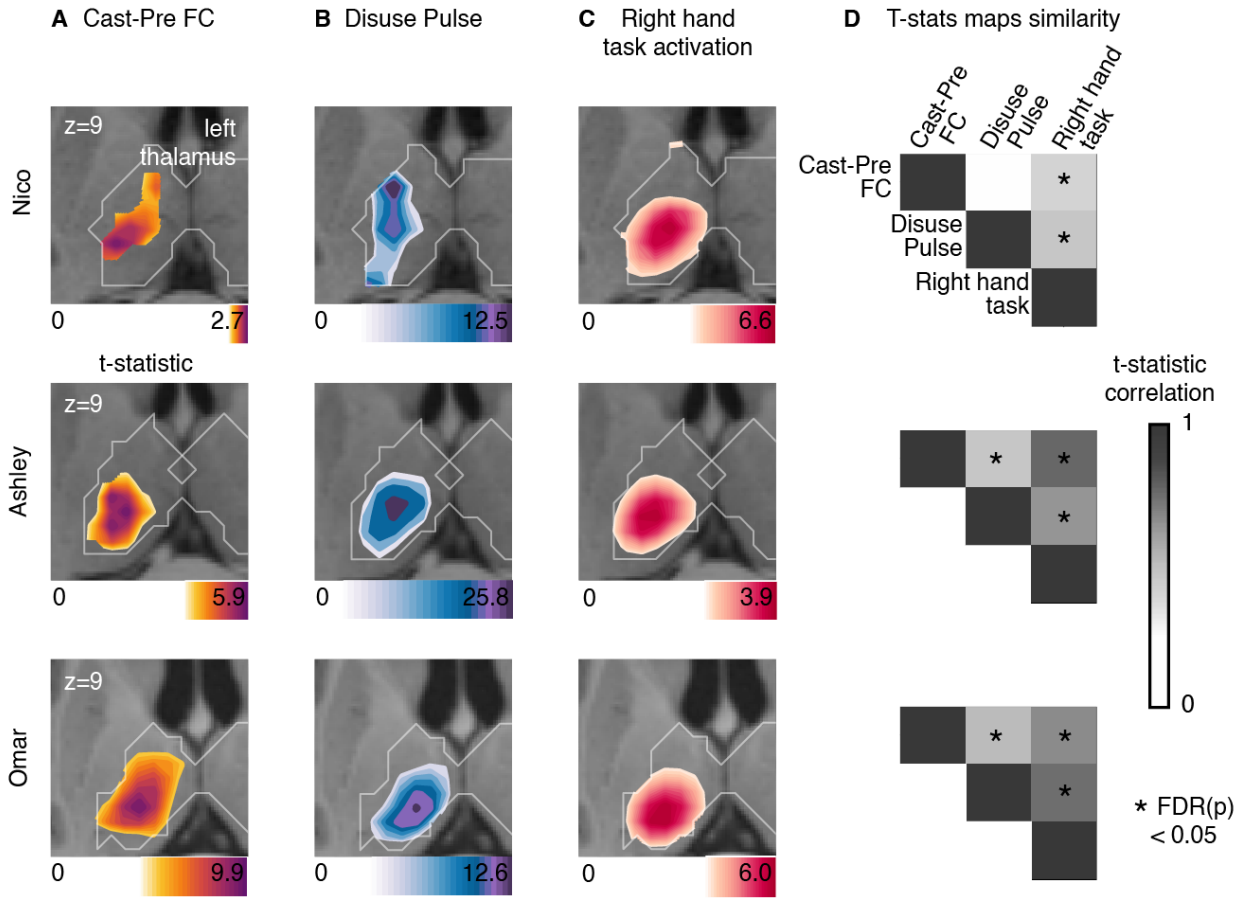

Figure 4: Thalamus representations of disuse-driven FC changes, pulses and hand movement task fMRI activations. *(A) Map of disuse-driven increases in FC with left $SM1_{ue}$ ROI (top 30th percentile t statistics). (B) Map of disuse pulses (top 30th percentile t statistics). (C) Map of right hand movement vs baseline task fMRI (HCP motor task; pre-cast; top 30th percentile t statistics). For all three maps, color scales are represented at the bottom of the map with maximum value at 99.5th percentile. (D) Correlation between left thalamic t statistic maps for disuse-driven FC increases, pulse and activation during hand movement (right hand vs baseline). Correlations between*

*unthresholded t statistics maps were tested against individual-specific null distribution effects for each participant (top to bottom : Nico, Ashley, Omar). Reported significant p < 0.05 corrected for FDR (black *).*

To assess whether the subcortical plasticity effects, indexed by FC changes, and disuse pulses coincided with the regions active during upper extremity movement, we analyzed motor task fMRI data collected at baseline (Figures 4,5). The HCP motor task is a simple motor effector localizer for hand, tongue and foot. Its block design is very potent and produced standard motor activation in the cortex over the central sulcus for all conditions (see Figure S7-10)

In the thalamus (Figure 4), all three participants showed task fMRI activations centrally. The task activations overlapped with the FC changes and the disuse pulses in each participant. This similarity was confirmed by the strength of correlation between t statistic maps, showing significant similarity against spatial null distributions (see Methods, Figure 4 D). Nico's peak FC change and disuse pulse in the thalamus showed more variability but stayed within the spread of right hand movement representations. Overall, thalamic FC changes and disuse pulses were similar to the right hand movement execution.

In order to gain a deeper insight into the thalamic distribution of both plasticity effects and the effector specific motor circuitry, we quantified the average t-statistic values within each thalamic nucleus (Figure S4,S5, individual THOMAS atlas segmentation, see Method). Thalamic nuclei showing the greatest plasticity effects were the centro-median (CM), the ventroposterior lateral (VPL) and ventral intermediate (VIM) (see Figure S6 for all participants). Right hand movement task activation showed consistent activation of CM, VPL, VIM across all participants. This set of nuclei remains specific when quantifying right > left hand movement, therefore showing movement laterality specificity (Figures S7-9). Thalamic nuclei representations between CM, VPL and VIM for disuse pulse and FC change show more variability across participants, highlighting difference in expression and reduced pattern similarity. Assuming some spatial variability due effect detectability in low signal area, the overall specificity of thalamic nuclei involved in plasticity effects validate the motor execution circuit integration.

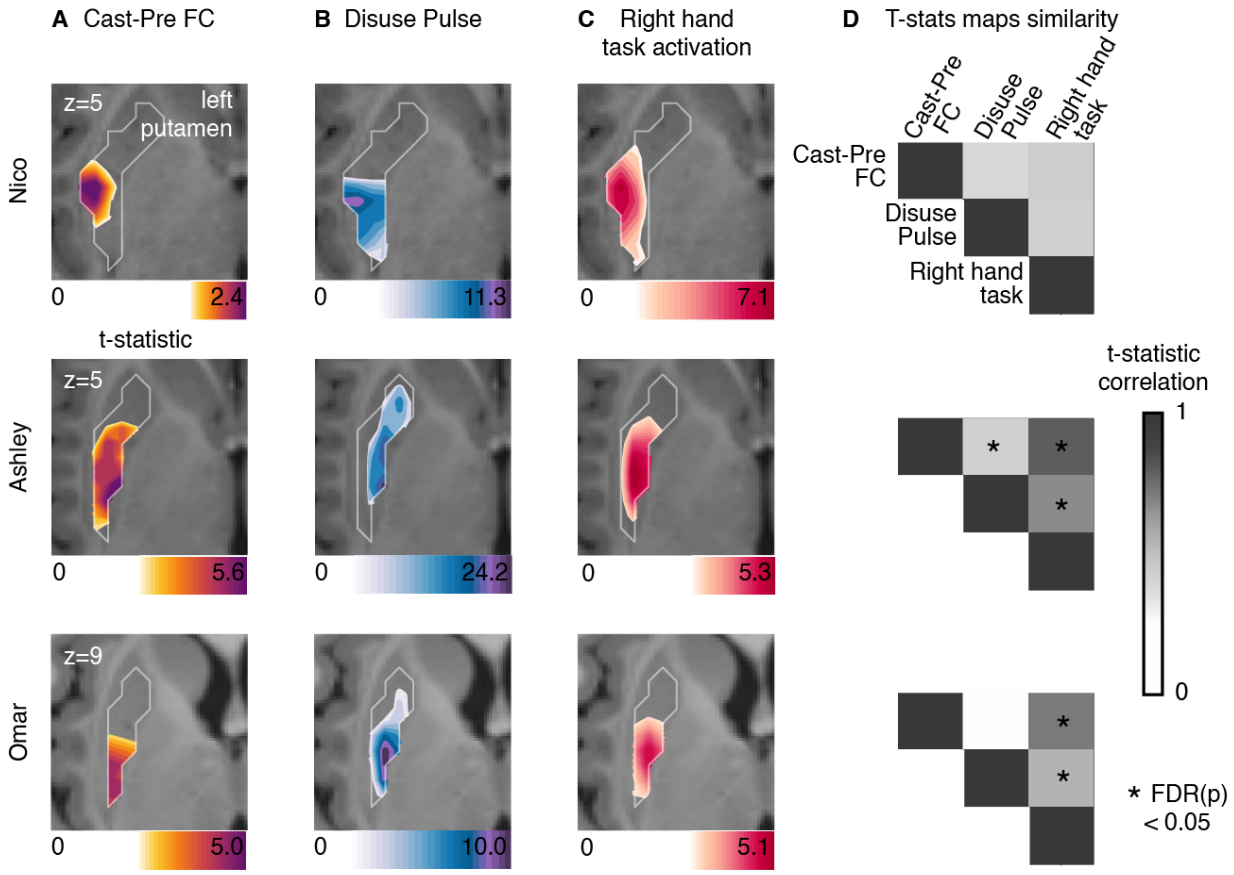

Figure 5: Putamen representations of disuse-driven FC changes, pulses and hand movement task fMRI activations. *(A) Map of disuse-driven increases in FC with left $SM1_{ue}$ ROI (top 30th percentile t statistics). (B) Map of disuse pulses (top 30th percentile t statistics). (C) Map of right hand movement vs baseline task fMRI (HCP motor task; pre-cast; top 30th percentile t statistics). For all three maps, color scales are represented at the bottom of the map with maximum value at 99.5th percentile. (D) Correlation between left putamen t statistic maps for disuse-driven FC increases, pulse and activation during hand movement (right hand vs baseline). Correlations between unthresholded t statistics maps were tested against individual-specific null distribution effects for each participant (top to bottom : Nico, Ashley, Omar). Reported significant $p < 0.05$ corrected for FDR (black *).*

In the putamen (Figure 5), all three participants showed task fMRI activations in the posterior section, as expected. The task activations overlapped with the FC changes and the disuse pulses in each participant. This similarity was confirmed by the strength of correlation between t statistic maps. Both Ashley and Omar showed significant similarities between the task fMRI, FC change and pulse maps, when tested using individual-specific null distributions (see Methods, Figure 4 D). Nico's peak FC change and disuse pulses in the thalamus showed spatial similarity with the right hand movement representations, however the rest of the thalamic map show differences in pattern that reduce their overall similarity. Putamen FC changes and disuse pulses representation were similar to the right hand movement execution.

Discussion

Disuse driven plasticity effects are not limited to cortex
Combining our individual-specific PFM approach (RSFC, task fMRI) with a potent plasticity intervention (upper extremity constraint by casting), and using analyses optimized for sensitivity, we observed significant subcortical FC changes and disuse pulses in the central thalamus (VIM, CM) and posterior putamen.These findings suggest that disuse can drive network changes at all levels: cortex, cerebellum, thalamus and striatum. In the cortex, the SCAN regions do not show an increase in FC or pulse presence across participants. While the SCAN is hypothesized to be the intermediate network in the CON to motor effector pathway, the lack of cortical involvement suggests that the plasticity integration between CON and motor effector is performed by other structures, potentially the cortico-striato-thalamic loop. Throughout the full depth of the motor and action control circuits, as verified by task fMRI activations, FC increases partially overlapped with the presence of disuse pulses, suggesting that they might represent a brain-wide plasticity mechanism. Since the overlap between pulses and FC increases was only partial and we previously demonstrated that regressing the disuse pulse does not fully explain the changes in FC[13], these findings reinforce the idea that disuse pulses represent one of several plasticity mechanisms that can alter FC.

Disuse strengthens FC in motor and action sub-circuitry
Increased FC between subcortical and cortical motor regions, in the presence of pulses, is consistent with our previously reported finding of strengthened FC between motor cortex and the CON [13]. However, these results cannot be fully accounted for by a simple Hebbian-like process [35,44,45], which one would predict should weaken FC in the setting of disuse (not firing together). Instead, it seems that pulses, by creating co-activation in the disused motor control circuit, help maintain the integrity of disused subcircuits [14], including their subcortical components. It seems plausible that maintained and even strengthened FC in the disused subcircuits enabled the rapid recovery of both behavior (actigraphy) and functional connectivity (within days) after cast removal [14].

Prior work in animal models suggests that neural adaptation to change in stimuli will start with a reduction of activity of inhibitory interneurons at the population level [33,46–48] , increasing the excitatory population activity, which in turn could increase the likelihood of spontaneous activity pulses. Reduced inhibition could also increase FC beyond the triggering of disuse pulses, since a rise in baseline neural activity can increase shared signal between regions.

Disuse-driven plasticity affects posterior putamen involved in habit formation
Rapid, goal-directed learning is thought to primarily involve the dorsomedial striatum, including the caudate, whereas the slower acquisition of habits, which are insensitive to changes in the reward value of the outcome, is thought to depend more on the dorsolateral striatum, including the posterior putamen [48–51]. The increased FC with the posterior putamen suggests that it might specifically be related to protecting existing motor skills. Indeed, our participants showed progressive decline of upper extremity movements throughout casting, which lasted 1-2 days after cast removal, suggesting

that participants learned to suppress movements of the casted arm. However, no fine motor or coordination motor impairment the day of cast removal.[14]

Plasticity in thalamic nuclei for motor, somatosensory and arousal

The central thalamus is important for motor and action execution and studies have tied movement performance to activity in VIM, VPL and CM thalamic nuclei [3,52], which is consistent with our motor task fMRI activations (Figure S4, S5, S7-9). The VIM is part of the thalamic ventro-lateral region (VL), primarily involved in motor control and relays information between the basal ganglia, cerebellum and motor cortex, whereas the VPL is part of the somatosensory system and relays sensory information related to touch, temperature, and pain from the body to the primary somatosensory cortex [53–55]. VIM is a common and effective DBS target for tremor. In cases of neurological injury or disease, such as stroke or neurodegenerative disorders, the VIM can undergo plasticity as part of the brain's adaptation and recovery mechanisms [32,56]. In rats, for example, VIM stroke results in specific skilled locomotor impairment (e.g., impaired ladder mobility, but not flat walk) [57]. Reorganization of activity in VIM after the stroke correlates with restored mobility [58,59]. In fact, successful movement performance, such as walking on a complex surface, after a VIM partial lesion are compensated within a few days, showing the highly effective plasticity of the thalamus [57]. Plastic reorganization can also occur in response to motor demands driving functional adaptation. For example, in humans, in the context of amputation, one study observed changes in the representation of the affected body parts within the VIM. Electrophysiological recording in a patient with arm amputation and long term use of a prosthetic has shown an enlargement of the shoulder representation in the VIM, which now is used for prosthetic grip control by the patient [32].

In addition to the VIM and VPL, the CM also showed FC increases, pulses and task fMRI activation. While the VIM is the DBS target of choice for tremor, the CM is being targeted in Tourette's and with increasing frequency also in epilepsy and disorders of consciousness [60], since it seems to play a special role in regulating arousal [61].

Thalamic plasticity pulses could carry local sleep spindles

The thalamus regulates sleep stages and slow oscillations in deep sleep [41]. Sleep events like thalamo-cortical spindles are thought to help memory and skill consolidation [62–64]. During deep sleep, slow waves of activity are observed across the cortex and relayed in the thalamus [65]. These slow waves are thought to help with homeostasis of neural activity after a day of novel experiences [44,66,67] . The slow waves help networks to synchronize and increase phase locked communication between regions [68,69].

The occurrence of disuse pulses in the central thalamus, most reliably in the CM, raises the question whether they might be related to thalamocortical sleep spindles. Could the disuse pulses represent a circuit-specific, sleep-like phenomenon happening during the awake resting-state? Indeed, local sleep can be observed during wakefulness [70]. After a long period in an awake state, EEG recordings in awake rats can capture local 'offline' stages similar to sleep, together with slow waves [71]. Consistent with this idea, the one participant who was always scanned in the morning (Nico) also had the lowest number of pulses. In contrast, Ashley and Omar were always scanned in the evening. Thus,

hours spent active since awakening could have driven the frequency of circuit-specific spontaneous activity pulses at the time of scanning.

Cortico-striato-thalamic FC increase as a marker of Disuse in Parkinson's Disease
Motor impairments in Parkinson's disease include tremor, rigidity and bradykinesia, and follow the loss of dopamine neurons projecting onto the caudate and putamen [2]. Motor impairments in Parkinson's are multiple and encompass tremor, rigidity and bradykinesia. In the thalamus, VIM is used as a target for DBS treatment of tremor. Electrophysiological studies in patients with Parkinson's diseaseparkinsonian mouse models have revealed increased beta power and prolongation of beta burst discharges propagating throughout cortico-basal basal ganglia circuits [72–75]. These beta bursts disappear when moving or with L-dopa treatment [76–78]. Secondarily, Parkinson's patients show an increase in FC between putamen, central thalamus and supplementary motor area, especially during akinesia [79–82]. In our arm immobilization paradigm, we observed similar increases in FC in the disused motor circuit, but after removing the cast, these FC changes reversed rapidly and motor behavior was unimpaired[13]. However, slow adaptation to not using their casted arm was observed[14] . If increased FC in the motor and action circuits is a marker of normal motor program updating, its detection in patients with Parkinson's disease may be a normal response to disuse and not a cause of parkinsonism [83,84]. Further research is needed to determine whether beta bursts detected with electrophysiology are related or similar to disuse pulses observable with fMRI.

Plasticity and stability in subcortex
Disuse-driven FC changes and spontaneous activity pulses are not confined to the cortex but extend into the putamen and central thalamus (VIM, CM, VPL). The anatomical pattern, especially the prominence of the CM evokes parallels to sleep-related mechanisms of consolidation and plasticity, as well the beta bursts seen in Parkinson's patients in the off state. These findings open up intriguing new avenues for studying disorders such as Parkinson's disease and sleep physiology. They also raise the interesting possibility that the mechanisms for changing the brain and for maintaining it are one and the same.

Methods

Human participants: We used a previously published dataset that comprised three healthy adult volunteers. The first participant (Nico) was 35 y old at the time of scanning and is male. The second participant (Ashley) was 25 y old and female. The third participant (Omar) was 27 years old and male. All participants were right-handed, as assessed by the Edinburgh Handedness Inventory [85] (Nico: +100, right handed; Ashley: +91, right-handed; Omar: +60, right-handed). The Washington University School of Medicine Institutional Review Board approved the study protocol and provided experimental oversight. Participants provided informed consent for all aspects of the study and were paid for their participation.

Experimental setup: Arm immobilization was conducted by constraining the participant's dominant (right) arm for two weeks (cast period). The immobilization followed a two weeks experimental baseline setup without constrained (pre cast period) and was followed by a recovery period of two weeks (post cast period). For one participant (Nico), the pre cast period was acquired one month before the cast period and data was consistently acquired at 5AM, while the two other participants were acquired at 9PM. For one participant (Omar), the cast was removed and recreated after one day of the cast period to adjust for finger comfort. Details of cast construction are described in Newbold et al. [14]

Imaging data: On each day of the experiment, a scan session was conducted to acquire structural and functional data. Structural MRI was consisted of four T1-weighted images (sagittal acquisition, 0.8 mm isotropic resolution, 3D MP-RAGE, Gradient echo) and four T2-weigthed images (sagittal acquisition, 0.8 mm isotropic resolution, 3D T2-SPC, Spin echo). A 30 minute rs-fMRI run was acquired during each session, and two runs of the HCP Motor strip mapping task [86,87] were acquired for each pre and post cast session. Ashley and Omar's functional data acquisition parameters used a higher quality data sequence than Nico's functional data (all 2D Gradient echo, echo planar, TR: 1.1 vs 2.2 seconds, 2.6 vs 4 mm isotropic resolution). All data were resampled at 3mm. Acquisition parameters and procedures are detailed in Newbold et al. [14].

Precision functional analysis: All following data processing and analysis is conducted at the participant level using its own defined functional and anatomical boundaries. All testing is done with null distribution built within-subject. All results are replicated across all participants and shown in figure for all three or for an exemplar participant.

MR Image Processing. Preprocessing of structural and functional images, denoising of rs-fMRI data, and cortical surface projection were performed previously [14]. Functional image processing followed a previously published pipeline [88] and involved temporal interpolation to correct for differences in slice acquisition timing, rigid-body correction of head movements, correction for susceptibility inhomogeneity-related distortions, and alignment to atlas space (711-2b implementation of Talairach space). For cortical projection and creation of cifti images, individual-specific surfaces were created defining the cortical gray-matter boundaries derived from T1-weighted images using FreeSurfer [89]. Subcortical boundaries from the Freesurfer segmentation were used to select voxels of interest for building the volume part of the cifti image. There were no systematic differences in head movement (mean FD or number of frames removed) between experimental conditions.

rs-fMRI and task-fMRI data denoising were different to reflect sensitivity to the type of analysis done later on the data:

rs-fMRI data denoising involved replacement of high-motion frames (framewise displacement [FD] > 0.1 mm) by temporal linear interpolation, band-pass filtering (0.005 to 0.1 Hz), and regression of nuisance time series, including head movement parameters, the global signal averaged across all gray-matter voxels, and orthogonalized waveforms extracted from ventricles, white matter, and extracranial tissues. The rs-fMRI for functional connectivity is then projected to cortical surface as the last step and smoothed using a two-dimensional 6-mm full-width half-maximum (FWHM) smoothing kernel and volume data were smoothed using a three-dimensional 4.7-mm FWHM kernel.

For task based analysis involving modeling of Hemodynamic response function, i.e. rs-fMRI data used in the pulse spatio-temporal representation analyses and HCP task data, denoising of data involved high-pass filtering (0.1Hz) before surface projection and regression of nuisances time series (head movements parameters, individual high-motion frames). Nuisances regression was done at the surface and subcortical volume level within a GLM design. Cortical surface data were smoothed at the last stage of each analysis using a two-dimensional 6-mm full-width half-maximum (FWHM) smoothing kernel and volume data were smoothed using a three-dimensional 4.7-mm FWHM kernel.

Fully processed data are available in the Derivatives folder of the Cast-Induced Plasticity dataset in OpenNeuro (https://openneuro.org/datasets/ds002766).

Primary SomatoMotor upper extremity region of interest: The upper extremity SM1 region was defined at the level of each individual using a Task-based approach combined with automatic labeling by FreeSurfer. Details were previously described in Newbold et al. [14].

Individual network representation: A set of 18 canonical functional networks was defined for each participant using a graph theory-based community detection algorithm and anatomical priors [17](see figure S1), the Infomap algorithm [90](https://www.mapequation.org/) . This algorithm allocates vertices from the surface and voxels from the subcortical into communities. Subsequently, these communities were categorized based on their similarity to established group-average networks recently updated to include the SCAN [17,20]. The final cortical resting state networks were derived from the consensus network assignments obtained through aggregation across thresholds.

Thalamic nuclei segmentation using THOMAS: The Thalamus-Optimized Multi-Atlas Segmentation (THOMAS v 2.1) method, a promising approach for identifying nuclei, was employed [25]. The choice of THOMAS followed the latest consensus of nuclei naming and automatic segmentation algorithm improvement. We also aimed to interpret our results in relation to clinical application and needed a robust localization of VIM, which has been shown to co-localized with the segment labeled VLPv (Ventro-Lateral-Posterior ventral) using the THOMAS segmentation [27]. For the thalamic nuclei segmentation in our precision mapping participant, the hips_thomas.csh function from version 2.1 was utilized. This version has been validated exclusively for T1 acquisition [91] and is accessible through Docker (https://github.com/thalamicseg/thomas_new). The average T1 acquisition, generated for the registration of all functional data, was employed for this purpose. Nuclei were mapped into cifti format and the resolution of functional image (3mm) to quantify overlap between brain maps and thalamic nuclei.

rs-fMRI Functional connectivity (FC): Average BOLD time series were calculated for each individual specific vertices/voxels to construct a full brain FC for each rs-fMRI session. Seed FC was estimated as the average of FC maps for each voxel in the seed. Pre cast session seed FC were average to produce baseline FC across analysis.

rs-fMRI FC change and testing: For casting sessions comparison to baseline (Pre casting) sessions, the Cohen's d was calculated at each vertex. The Cohen's d translates into the effect size of the change in FC as it accounts for standard deviation of each set of sessions compared. This allows higher sensitivity to subcortical casting effects as the subcortical correlation values to the rest of the brain is lower but robust across sessions. The Cohen's d is also more stable to variation in the number of measurements between subjects or between phases compared to a

t-statistic. Due to repeated measure design, the sample size is small (only 14 data points in time per phase) and a loss of a single data point impacts the interpretation of t-statistic more than cohen's d. Because of the specific behavior of statistical metric in small sample size with subject specific variance compared to population study, we perform a within subject null hypothesis testing. To define significant effect, we computed a null distribution FC maps from randomizing sessions labels 1000 times and computed a multi threshold cluster based correction. 10 thresholds were defined from the 10th percentage from 0 to the maximum value of the true data. Cluster of data passing cluster size correction at $p<0.05$ for at least two thresholds are displayed in figure 1. Cluster size correction was estimated for each anatomical structure (cortical and subcortical) independently in order to adjust for biology constraints.

Pulse detection and modeling: The average BOLD time series for the Left SM1 were computed for each rs-fMRI. The average across all sessions of standard deviation of each time series and the standard deviation of the difference between Left and Right time series were computed to define the thresholds of pulse detection. A Left SM1 pulse is defined by two criteria. First criterion is an increase of Left to Right time series difference above 2.3 times the cross-session average standard deviation of the Left to Right time series difference. Second criterion is an increase in signal of Left SM1 time series above 2.3 times its cross-session average time series standard deviation. Additionally, pulses with a high correlation (>0.8) with head movement (on a 18s-window centered on the pulse peak) were removed to correct misdetection due to large co-fluctuation away from mean activity.

In order to study the subcortical pattern of the disuse pulse described in Newbold et al. [14], we perform a pulse detection analysis sensitive to potential differences in hemodynamic response function (HRF) shape [92] in subcortical regions. We model the HRF shape at each vertex and voxel of each pulses. To model the timing of peak activity during a pulse across the brain, a double gamma HRF function model from nipy (SPM based hrf double gamma, nipy.modalities.fmri.hrf) was used for each vertices and voxels of the brain using a model optimizer from scipy (scipy.optimize.curve_fit). Peak timing across each pulse map was aligned to the mean peak value of the Left SM1 region. We then used the number of pulses successfully modeled per voxels to select the most robust regions of pulse activity. The top 20% of frequent pulse activity is displayed in figure 2 where we display the average pulse peak delay from L SM1 reference. The displayed map was thresholded at 1.1 seconds (TR) after the Left SM1 pulse peak.

Motor Task analysis: Task block designs for each movement condition (Tongue, Left Hand, Right Hand, Left Foot, Right Foot) were modeled using a double gamma HRF in a GLM analysis from FSL feat. Onset and offset of block were modeled as an independent regressor [93]. Analysis was conducted independently on surface projection for each cortical hemisphere and in volume space for subcortical cortex, following the HCP pipeline steps (release v4.3) for each task run. Second level analysis across runs within participants was performed with FSl and the resulting Z-score were used to study thalamic nuclei activity during movement performance.

VIM localization: The voxels representing the possible VIM target were determined using the anterior commissure - posterior commissure (ACPC) formula [94]. The T1 was aligned on the ACPC line using ACPC detect [95]. We used the Freesurfer segmentation of the third ventricle for the following steps of planes range estimation of the VIM target location. The coronal range was estimated at 1/4 of the third ventricle length from the posterior limit of the ventricle with 2 mm anterior range. The sagittal range was estimated between 14 mm from the center of the third

ventricle and 11 mm from the border of the third ventricle. The voxels between the three axis range were brought to functional orientation and to the functional resolution of 3mm.

Quantification and testing of effects against individual null distribution: To test an effect against null, here specificity to a thalamic nuclei or similarity between maps, we aim to account for spatial distribution and dependency of the effect. We produce 1000 spatial random representations of the brain map of interest using Moran spectral randomization, an algorithm that gets informed by spatial distances between vertices [96,97]. The map generation focuses on the spatial structure of interest, here the left thalamus. This ensures that random effects related to nearby structure do not alter the specificity of the effect from the thalamus. We compute the values of interest, i.e. average values per nuclei or correlation across voxels of the thalamus and compare the true to the random null distribution data. Tests were corrected for multiple comparisons across subjects using false discovery rate.

Acknowledgments

This work was supported by NIH grants NS123345 (B.P.K.), NS098482 (B.P.K.),MH129616 (T.O.L.), T32DA007261 (S.R.K), MH096773 N.U.F.D.), MH122066 (N.U.F.D.), MH121276 (N.U.F.D.), MH124567 (N.U.F.D.), NS129521 (N.U.F.D.), and NS088590 (N.U.F.D.); by the Taylor Family Foundation (T.O.L.); by the Intellectual and Developmental Disabilities Research Center (N.U.F.D.); by the Kiwanis Foundation (N.U.F.D.); by the Washington University Hope Center for Neurological Disorders (B.P.K. and N.U.F.D.); and by Mallinckrodt Institute of Radiology pilot funding (N.U.F.D.). Computations were performed using the facilities of the Washington University Research Computing and Informatics Facility, which were partially funded by NIH grants S10OD025200, 1S10RR022984-01A1 and 1S10OD018091-01. Additional support is provided by the McDonnell Center for Systems Neuroscience.

Competing Interests

A.N.V. and N.U.F.D. have a financial interest in Turing Medical Inc. and may benefit financially if the company is successful in marketing FIRMM motion monitoring software products. A.N.V. and N.U.F.D. may receive royalty income based on FIRMM technology developed at Washington University School of Medicine and Oregon Health and Sciences University and licensed to Turing Medical Inc. D.A.F. and N.U.F.D. are co-founders of Turing Medical Inc. These potential conflicts of interest have been reviewed and are managed by Washington University School of Medicine, Oregon Health and Sciences University and the University of Minnesota. A.N.V. is now an employee of Turing Medical Inc. The other authors declare no competing interests.

Reference

1. von Bernhardi R, Bernhardi LE von, Eugenín J. What Is Neural Plasticity? In: von Bernhardi R, Eugenín J, Muller KJ, eds. *The Plastic Brain*. Advances in Experimental Medicine and Biology. Springer International Publishing; 2017:1-15. doi:10.1007/978-3-319-62817-2_1
2. Beitz JM. Parkinson's disease: a review. *Front Biosci Sch Ed*. 2014;6:65-74.
3. Opri E, Cernera S, Okun MS, Foote KD, Gunduz A. The Functional Role of Thalamocortical Coupling in the Human Motor Network. *J Neurosci*. 2019;39(41):8124-8134. doi:10.1523/JNEUROSCI.1153-19.2019
4. Ilyas A, Pizarro D, Romeo AK, Riley KO, Pati S. The centromedian nucleus: Anatomy, physiology, and clinical implications. *J Clin Neurosci*. 2019;63:1-7. doi:10.1016/j.jocn.2019.01.050
5. Van der Werf YD, Witter MP, Groenewegen HJ. The intralaminar and midline nuclei of the thalamus. Anatomical and functional evidence for participation in processes of arousal and awareness. *Brain Res Rev*. 2002;39(2):107-140. doi:10.1016/S0165-0173(02)00181-9
6. Bonelli RM, Cummings JL. Frontal-subcortical circuitry and behavior. *Dialogues Clin Neurosci*. 2007;9(2):141-151.
7. Bennett CM, Miller MB. How reliable are the results from functional magnetic resonance imaging? *Ann N Y Acad Sci*. 2010;1191(1):133-155. doi:10.1111/j.1749-6632.2010.05446.x
8. Maugeri L, Moraschi M, Summers P, et al. Assessing denoising strategies to increase signal to noise ratio in spinal cord and in brain cortical and subcortical regions. *J Instrum*. 2018;13(02):C02028. doi:10.1088/1748-0221/13/02/C02028
9. Appelbaum LG, Shenasa MA, Stolz L, Daskalakis Z. Synaptic plasticity and mental health: methods, challenges and opportunities. *Neuropsychopharmacology*. 2023;48(1):113-120. doi:10.1038/s41386-022-01370-w
10. Kolb B, Gibb R. Brain Plasticity and Behaviour in the Developing Brain. *J Can Acad Child Adolesc Psychiatry*. 2011;20(4):265-276.
11. Mateos-Aparicio P, Rodríguez-Moreno A. The Impact of Studying Brain Plasticity. *Front Cell Neurosci*. 2019;13. Accessed February 21, 2023. https://www.frontiersin.org/articles/10.3389/fncel.2019.00066
12. Newbold DJ, Dosenbach NU. Tracking plasticity of individual human brains. *Curr Opin Behav Sci*. 2021;40:161-168. doi:10.1016/j.cobeha.2021.04.018
13. Newbold DJ, Gordon EM, Laumann TO, et al. Cingulo-opercular control network and disused motor circuits joined in standby mode. *Proc Natl Acad Sci*. 2021;118(13):e2019128118. doi:10.1073/pnas.2019128118
14. Newbold DJ, Laumann TO, Hoyt CR, et al. Plasticity and Spontaneous Activity Pulses in Disused Human Brain Circuits. *Neuron*. 2020;107(3):580-589.e6. doi:10.1016/j.neuron.2020.05.007
15. Hubel DH, Wiesel TN. Receptive fields and functional architecture in two nonstriate visual areas (18 and 19) of the cat. *J Neurophysiol*. 1965;28(2):229-289.
16. Merzenich MM, Kaas JH, Wall J, Nelson RJ, Sur M, Felleman D. Topographic reorganization of somatosensory cortical areas 3b and 1 in adult monkeys following restricted deafferentation. *Neuroscience*. 1983;8(1):33-55. doi:10.1016/0306-4522(83)90024-6

17. Gordon EM, Laumann TO, Gilmore AW, et al. Precision Functional Mapping of Individual Human Brains. *Neuron*. 2017;95(4):791-807.e7. doi:10.1016/j.neuron.2017.07.011
18. Dosenbach NUF, Fair DA, Cohen AL, Schlaggar BL, Petersen SE. A dual-networks architecture of top-down control. *Trends Cogn Sci*. 2008;12(3):99-105. doi:10.1016/j.tics.2008.01.001
19. D'Andrea CB, Laumann TO, Newbold DJ, et al. Substructure of the brain's Cingulo-Opercular network. Published online October 10, 2023:2023.10.10.561772. doi:10.1101/2023.10.10.561772
20. Gordon EM, Chauvin RJ, Van AN, et al. A somato-cognitive action network alternates with effector regions in motor cortex. *Nature*. 2023;617(7960):351-359. doi:10.1038/s41586-023-05964-2
21. Lanciego JL, Luquin N, Obeso JA. Functional Neuroanatomy of the Basal Ganglia. *Cold Spring Harb Perspect Med*. 2012;2(12):a009621. doi:10.1101/cshperspect.a009621
22. Jahanshahi M, Obeso I, Rothwell JC, Obeso JA. A fronto-striato-subthalamic-pallidal network for goal-directed and habitual inhibition. *Nat Rev Neurosci*. 2015;16(12):719-732. doi:10.1038/nrn4038
23. Pekny SE, Izawa J, Shadmehr R. Reward-Dependent Modulation of Movement Variability. *J Neurosci*. 2015;35(9):4015-4024. doi:10.1523/JNEUROSCI.3244-14.2015
24. Rae CL, Hughes LE, Anderson MC, Rowe JB. The Prefrontal Cortex Achieves Inhibitory Control by Facilitating Subcortical Motor Pathway Connectivity. *J Neurosci*. 2015;35(2):786-794. doi:10.1523/JNEUROSCI.3093-13.2015
25. Su JH, Thomas FT, Kasoff WS, et al. Thalamus Optimized Multi Atlas Segmentation (THOMAS): fast, fully automated segmentation of thalamic nuclei from structural MRI. *NeuroImage*. 2019;194:272-282. doi:10.1016/j.neuroimage.2019.03.021
26. Mai JK, Majtanik M. Toward a Common Terminology for the Thalamus. *Front Neuroanat*. 2019;12. Accessed November 2, 2023. https://www.frontiersin.org/articles/10.3389/fnana.2018.00114
27. Su JH, Choi EY, Tourdias T, et al. Improved Vim targeting for focused ultrasound ablation treatment of essential tremor: A probabilistic and patient-specific approach. *Hum Brain Mapp*. 2020;41(17):4769-4788. doi:10.1002/hbm.25157
28. Bertino S, Basile GA, Bramanti A, et al. Ventral intermediate nucleus structural connectivity-derived segmentation: anatomical reliability and variability. *NeuroImage*. 2021;243:118519. doi:10.1016/j.neuroimage.2021.118519
29. Fama R, Sullivan EV. Thalamic structures and associated cognitive functions: Relations with age and aging. *Neurosci Biobehav Rev*. 2015;54:29-37. doi:10.1016/j.neubiorev.2015.03.008
30. Shine JM, Lewis LD, Garrett DD, Hwang K. The impact of the human thalamus on brain-wide information processing. *Nat Rev Neurosci*. 2023;24(7):416-430. doi:10.1038/s41583-023-00701-0
31. Mai JK, Majtanik M. Toward a Common Terminology for the Thalamus. *Front Neuroanat*. 2019;12:114. doi:10.3389/fnana.2018.00114
32. Whatley BP, Chopek JW, Hill R, Brownstone RM. Case Studies in Neuroscience: Evidence of motor thalamus reorganization following bilateral forearm amputations.

J Neurophysiol. 2018;120(4):1776-1780. doi:10.1152/jn.00120.2018
33. Froemke RC. Plasticity of Cortical Excitatory-Inhibitory Balance. *Annu Rev Neurosci*. 2015;38:195-219. doi:10.1146/annurev-neuro-071714-034002
34. Avoli M, de Curtis M, Gnatkovsky V, et al. Specific imbalance of excitatory/inhibitory signaling establishes seizure onset pattern in temporal lobe epilepsy. *J Neurophysiol*. 2016;115(6):3229-3237. doi:10.1152/jn.01128.2015
35. Dehghani N, Peyrache A, Telenczuk B, et al. Dynamic Balance of Excitation and Inhibition in Human and Monkey Neocortex. *Sci Rep*. 2016;6(1):23176. doi:10.1038/srep23176
36. Toader O, Forte N, Orlando M, et al. Dentate gyrus network dysfunctions precede the symptomatic phase in a genetic mouse model of seizures. *Front Cell Neurosci*. 2013;7:138. doi:10.3389/fncel.2013.00138
37. Rupert DD, Shea SD. Parvalbumin-Positive Interneurons Regulate Cortical Sensory Plasticity in Adulthood and Development Through Shared Mechanisms. *Front Neural Circuits*. 2022;16:886629. doi:10.3389/fncir.2022.886629
38. Yang JC, Bullinger KL, Isbaine F, et al. Centromedian thalamic deep brain stimulation for drug-resistant epilepsy: single-center experience. *J Neurosurg*. 2022;137(6):1591-1600. doi:10.3171/2022.2.JNS212237
39. Cukiert A, Cukiert CM, Burattini JA, Mariani PP. Seizure outcome during bilateral, continuous, thalamic centromedian nuclei deep brain stimulation in patients with generalized epilepsy: a prospective, open-label study. *Seizure*. 2020;81:304-309. doi:10.1016/j.seizure.2020.08.028
40. Agashe S, Burkholder D, Starnes K, et al. Centromedian Nucleus of the Thalamus Deep Brain Stimulation for Genetic Generalized Epilepsy: A Case Report and Review of Literature. *Front Hum Neurosci*. 2022;16. Accessed August 24, 2023. https://www.frontiersin.org/articles/10.3389/fnhum.2022.858413
41. Schreiner T, Kaufmann E, Noachtar S, Mehrkens JH, Staudigl T. The human thalamus orchestrates neocortical oscillations during NREM sleep. *Nat Commun*. 2022;13(1):5231. doi:10.1038/s41467-022-32840-w
42. Timofeev I, Chauvette S. The Spindles: Are They Still Thalamic? *Sleep*. 36(6):825. doi:10.5665/sleep.2702
43. Bastuji H, Lamouroux P, Villalba M, Magnin M, Garcia-Larrea L. Local sleep spindles in the human thalamus. *J Physiol*. 2020;598(11):2109-2124. doi:10.1113/JP279045
44. Turrigiano GG. The Self-Tuning Neuron: Synaptic Scaling of Excitatory Synapses. *Cell*. 2008;135(3):422-435. doi:10.1016/j.cell.2008.10.008
45. Fox K, Stryker M. Integrating Hebbian and homeostatic plasticity: introduction. *Philos Trans R Soc B Biol Sci*. 2017;372(1715):20160413. doi:10.1098/rstb.2016.0413
46. Mackwood O, Naumann LB, Sprekeler H. Learning excitatory-inhibitory neuronal assemblies in recurrent networks. Palmer SE, Ivry RB, eds. *eLife*. 2021;10:e59715. doi:10.7554/eLife.59715
47. Bannon NM, Chistiakova M, Volgushev M. Synaptic Plasticity in Cortical Inhibitory Neurons: What Mechanisms May Help to Balance Synaptic Weight Changes? *Front Cell Neurosci*. 2020;14. Accessed August 31, 2022. https://www.frontiersin.org/articles/10.3389/fncel.2020.00204
48. Yin HH, Knowlton BJ. The role of the basal ganglia in habit formation. *Nat Rev*

Neurosci. 2006;7(6):464-476. doi:10.1038/nrn1919
49. Balleine BW, Delgado MR, Hikosaka O. The role of the dorsal striatum in reward and decision-making. *J Neurosci Off J Soc Neurosci*. 2007;27(31):8161-8165. doi:10.1523/JNEUROSCI.1554-07.2007
50. Turner KM, Svegborn A, Langguth M, McKenzie C, Robbins TW. Opposing Roles of the Dorsolateral and Dorsomedial Striatum in the Acquisition of Skilled Action Sequencing in Rats. *J Neurosci*. 2022;42(10):2039-2051. doi:10.1523/JNEUROSCI.1907-21.2022
51. Vandaele Y, Mahajan NR, Ottenheimer DJ, Richard JM, Mysore SP, Janak PH. Distinct recruitment of dorsomedial and dorsolateral striatum erodes with extended training. *eLife*. 8:e49536. doi:10.7554/eLife.49536
52. Charyasz E, Heule R, Molla F, et al. Functional mapping of sensorimotor activation in the human thalamus at 9.4 Tesla. *Front Neurosci*. 2023;17:1116002. doi:10.3389/fnins.2023.1116002
53. Vázquez-García M, Wallman MJ, Timofeev I. Somatotopic organization of ferret thalamus. *Front Integr Neurosci*. 2014;8:90. doi:10.3389/fnint.2014.00090
54. Kaas JH, Nelson RJ, Sur M, Dykes RW, Merzenich MM. The somatotopic organization of the ventroposterior thalamus of the squirrel monkey, Saimiri sciureus. *J Comp Neurol*. 1984;226(1):111-140. doi:10.1002/cne.902260109
55. Hong JH, Kwon HG, Jang SH. Probabilistic Somatotopy of the Spinothalamic Pathway at the Ventroposterolateral Nucleus of the Thalamus in the Human Brain. *Am J Neuroradiol*. 2011;32(7):1358-1362. doi:10.3174/ajnr.A2497
56. Beloozerova IN. Neuronal activity reorganization in motor cortex for successful locomotion after a lesion in the ventrolateral thalamus. *J Neurophysiol*. 2022;127(1):56-85. doi:10.1152/jn.00191.2021
57. Beloozerova IN. Neuronal activity reorganization in motor cortex for successful locomotion after a lesion in the ventrolateral thalamus. *J Neurophysiol*. 2022;127(1):56-85. doi:10.1152/jn.00191.2021
58. Favre I, Zeffiro TA, Detante O, Krainik A, Hommel M, Jaillard A. Upper limb recovery after stroke is associated with ipsilesional primary motor cortical activity: a meta-analysis. *Stroke*. 2014;45(4):1077-1083. doi:10.1161/STROKEAHA.113.003168
59. Ward NS, Brown MM, Thompson AJ, Frackowiak RSJ. Neural correlates of outcome after stroke: a cross-sectional fMRI study. *Brain J Neurol*. 2003;126(Pt 6):1430-1448. doi:10.1093/brain/awg145
60. Arnts H, Coolen SE, Fernandes FW, et al. The intralaminar thalamus: a review of its role as a target in functional neurosurgery. *Brain Commun*. 2023;5(3):fcad003. doi:10.1093/braincomms/fcad003
61. Gottshall JL, Adams ZM, Forgacs PB, Schiff ND. Daytime Central Thalamic Deep Brain Stimulation Modulates Sleep Dynamics in the Severely Injured Brain: Mechanistic Insights and a Novel Framework for Alpha-Delta Sleep Generation. *Front Neurol*. 2019;10:20. doi:10.3389/fneur.2019.00020
62. Latchoumane CFV, Ngo HVV, Born J, Shin HS. Thalamic Spindles Promote Memory Formation during Sleep through Triple Phase-Locking of Cortical, Thalamic, and Hippocampal Rhythms. *Neuron*. 2017;95(2):424-435.e6. doi:10.1016/j.neuron.2017.06.025

63. Hahn MA, Heib D, Schabus M, Hoedlmoser K, Helfrich RF. Slow oscillation-spindle coupling predicts enhanced memory formation from childhood to adolescence. Haegens S, Colgin LL, eds. *eLife*. 2020;9:e53730. doi:10.7554/eLife.53730
64. Klinzing JG, Mölle M, Weber F, et al. Spindle activity phase-locked to sleep slow oscillations. *NeuroImage*. 2016;134:607-616. doi:10.1016/j.neuroimage.2016.04.031
65. Gent TC, Bassetti CL, Adamantidis AR. Sleep-wake control and the thalamus. *Curr Opin Neurobiol*. 2018;52:188-197. doi:10.1016/j.conb.2018.08.002
66. Frank MG. Erasing synapses in sleep: is it time to be SHY? *Neural Plast*. 2012;2012:264378. doi:10.1155/2012/264378
67. Tononi G, Cirelli C. Sleep and the Price of Plasticity: From Synaptic and Cellular Homeostasis to Memory Consolidation and Integration. *Neuron*. 2014;81(1):12-34. doi:10.1016/j.neuron.2013.12.025
68. Esser SK, Hill SL, Tononi G. Sleep Homeostasis and Cortical Synchronization: I. Modeling the Effects of Synaptic Strength on Sleep Slow Waves. *Sleep*. 2007;30(12):1617-1630.
69. Guo D, Thomas RJ, Liu Y, Shea SA, Lu J, Peng CK. Slow wave synchronization and sleep state transitions. *Sci Rep*. 2022;12(1):7467. doi:10.1038/s41598-022-11513-0
70. Lewis LD. The interconnected causes and consequences of sleep in the brain. *Science*. 2021;374(6567):564-568. doi:10.1126/science.abi8375
71. Vyazovskiy VV, Olcese U, Hanlon EC, Nir Y, Cirelli C, Tononi G. Local sleep in awake rats. *Nature*. 2011;472(7344):443-447. doi:10.1038/nature10009
72. Tai CH. Subthalamic burst firing: A pathophysiological target in Parkinson's disease. *Neurosci Biobehav Rev*. 2022;132:410-419. doi:10.1016/j.neubiorev.2021.11.044
73. Cagnan H, Mallet N, Moll CKE, et al. Temporal evolution of beta bursts in the parkinsonian cortical and basal ganglia network. *Proc Natl Acad Sci*. 2019;116(32):16095-16104. doi:10.1073/pnas.1819975116
74. West TO, Berthouze L, Halliday DM, et al. Propagation of beta/gamma rhythms in the cortico-basal ganglia circuits of the parkinsonian rat. *J Neurophysiol*. 2018;119(5):1608-1628. doi:10.1152/jn.00629.2017
75. Sharott A, Vinciati F, Nakamura KC, Magill PJ. A Population of Indirect Pathway Striatal Projection Neurons Is Selectively Entrained to Parkinsonian Beta Oscillations. *J Neurosci Off J Soc Neurosci*. 2017;37(41):9977-9998. doi:10.1523/JNEUROSCI.0658-17.2017
76. Torrecillos F, Tinkhauser G, Fischer P, et al. Modulation of Beta Bursts in the Subthalamic Nucleus Predicts Motor Performance. *J Neurosci*. 2018;38(41):8905-8917. doi:10.1523/JNEUROSCI.1314-18.2018
77. Vinding MC, Tsitsi P, Waldthaler J, et al. Reduction of spontaneous cortical beta bursts in Parkinson's disease is linked to symptom severity. *Brain Commun*. 2020;2(1):fcaa052. doi:10.1093/braincomms/fcaa052
78. Ray NJ, Jenkinson N, Wang S, et al. Local field potential beta activity in the subthalamic nucleus of patients with Parkinson's disease is associated with improvements in bradykinesia after dopamine and deep brain stimulation. *Exp Neurol*. 2008;213(1):108-113. doi:10.1016/j.expneurol.2008.05.008
79. Albano L, Agosta F, Basaia S, et al. Functional connectivity in Parkinson's disease candidates for deep brain stimulation. *Npj Park Dis*. 2022;8(1):1-12. doi:10.1038/s41531-021-00268-6

80. Hensel L, Hoffstaedter F, Caspers J, et al. Functional Connectivity Changes of Key Regions for Motor Initiation in Parkinson's Disease. *Cereb Cortex N Y NY*. 2019;29(1):383-396. doi:10.1093/cercor/bhy259
81. Gao L lin, Wu T. The study of brain functional connectivity in Parkinson's disease. *Transl Neurodegener*. 2016;5(1):18. doi:10.1186/s40035-016-0066-0
82. Owens-Walton C, Jakabek D, Power BD, et al. Increased functional connectivity of thalamic subdivisions in patients with Parkinson's disease. *PLOS ONE*. 2019;14(9):e0222002. doi:10.1371/journal.pone.0222002
83. Wichmann T. Changing views of the pathophysiology of Parkinsonism. *Mov Disord Off J Mov Disord Soc*. 2019;34(8):1130-1143. doi:10.1002/mds.27741
84. Cheung THC, Ding Y, Zhuang X, Kang UJ. Learning critically drives parkinsonian motor deficits through imbalanced striatal pathway recruitment. *Proc Natl Acad Sci*. 2023;120(12):e2213093120. doi:10.1073/pnas.2213093120
85. Oldfield RC. The assessment and analysis of handedness: The Edinburgh inventory. *Neuropsychologia*. 1971;9(1):97-113. doi:10.1016/0028-3932(71)90067-4
86. Barch DM, Burgess GC, Harms MP, et al. Function in the human connectome: Task-fMRI and individual differences in behavior. *NeuroImage*. 2013;80:169-189. doi:10.1016/j.neuroimage.2013.05.033
87. Bizzi A, Blasi V, Falini A, et al. Presurgical functional MR imaging of language and motor functions: Validation with intraoperative electrocortical mapping. *Radiology*. 2008;248(2):579-589. doi:10.1148/radiol.2482071214
88. Raut RV, Mitra A, Snyder AZ, Raichle ME. On time delay estimation and sampling error in resting-state fMRI. *NeuroImage*. 2019;194:211-227. doi:10.1016/j.neuroimage.2019.03.020
89. Fischl B. FreeSurfer. *NeuroImage*. 2012;62(2):774-781. doi:10.1016/j.neuroimage.2012.01.021
90. Rosvall M, Bergstrom CT. Maps of random walks on complex networks reveal community structure. *Proc Natl Acad Sci U S A*. 2008;105(4):1118-1123. doi:10.1073/pnas.0706851105
91. Pfefferbaum A, Sullivan EV, Zahr NM, Pohl KM, Saranathan M. Multi-atlas thalamic nuclei segmentation on standard T1-weighed MRI with application to normal aging. *Hum Brain Mapp*. 2023;44(2):612-628. doi:10.1002/hbm.26088
92. Bielczyk NZ, Llera A, Buitelaar JK, Glennon JC, Beckmann CF. The impact of hemodynamic variability and signal mixing on the identifiability of effective connectivity structures in BOLD fMRI. *Brain Behav*. 2017;7(8):n/a-n/a. doi:10.1002/brb3.777
93. Dosenbach NUF, Visscher KM, Palmer ED, et al. A core system for the implementation of task sets. *Neuron*. 2006;50(5):799-812. doi:10.1016/j.neuron.2006.04.031
94. Acar F, Miller JP, Berk MC, Anderson G, Burchiel KJ. Safety of anterior commissure-posterior commissure-based target calculation of the subthalamic nucleus in functional stereotactic procedures. *Stereotact Funct Neurosurg*. 2007;85(6):287-291. doi:10.1159/000107361
95. Ardekani BA, Bachman AH. Model-based automatic detection of the anterior and posterior commissures on MRI scans. *NeuroImage*. 2009;46(3):677-682. doi:10.1016/j.neuroimage.2009.02.030

96. Markello RD, Misic B. Comparing spatial null models for brain maps. *NeuroImage*. 2021;236:118052. doi:10.1016/j.neuroimage.2021.118052
97. Markello RD, Hansen JY, Liu ZQ, et al. neuromaps: structural and functional interpretation of brain maps. *Nat Methods*. Published online October 6, 2022:1-8. doi:10.1038/s41592-022-01625-w